

Design and field testing of a non-linear single-beam echosounder for multi-frequency seabed characterization

Irène Mopin ^{a,*}, Jacques Marchal ^b, Michel Legris ^a, Gilles Le Chenadec ^a, Philippe Blondel ^c, Benoît Zerr ^a

^a ENSTA Bretagne, UMR 6285, Lab-STICC, STIC-PRASYS, 2 rue François Verny, 29806 Brest Cedex 09, France

^b Sorbonne Université, UMR 7190, Institut Jean le Rond D'Alembert, 2 Place de la Gare de Ceinture, 78210 Saint Cyr L'École, France

^c University of Bath, Department of Physics, Claverton Down, Bath BA2 7AY, United Kingdom

ARTICLE INFO

Article history:

Received 19 February 2021

Received in revised form 1 July 2021

Accepted 21 October 2021

Available online 22 November 2021

Keywords:

Underwater acoustics

Non-linear acoustics

Backscatter strength (BS)

Seabed characterization

Single-beam echosounder (SBES)

ABSTRACT

Seabed mapping and characterization are best performed using several frequencies and several angles of incidence. This is often an issue because of the need to employ different sonars, with distinct frequencies but co-located as much as possible to image the same patch of seafloor. This article presents the design, calibration and field testing of a multiple-frequency single-beam echosounder (SBES), mounted on a mechanical pan-and-tilt head. It uses very high transmitting levels to produce non-linear effects and generate harmonics of a 100 kHz fundamental frequency. PZT transducers are used to transmit high acoustic powers and PDVF transducers enable the reception of scattering levels over a very broad frequency band (for the different harmonics). Tank experiments are used to verify effective harmonic generation. The shock distance (at which harmonics are at their maximum level) is measured as 2 m from the transmitter and recommended as the minimum far-field range. Non-linear transmission losses (distinct from linear losses) are calibrated using a full metal sphere 38.1 mm in diameter and of known frequency response, up to ranges commensurate with the depths expected in the field (≤ 30 m). The -3 dB beamwidth varies from 5.8° at 100 kHz to 2.8° at 300 kHz. Harmonics are used to resolve phase ambiguities in detecting seabed depths. Backscattering strengths *BS* are matched to the Generic Seafloor Acoustic Backscatter (GSAB) model to derive the best-fitting parameters. Field validation took place in the Bay of Brest (France) in May 2016, over three different types of seafloor (namely: sandy mud; gravel; gravelly coarse sand with maerl). Additional *in situ* calibration was used. The echosounder was pointed at angles from 0° (nadir) to 60° by 5° steps. One of the areas surveyed ("Carré Renard"), commonly used for instrument calibration and comparison with other measurements, showed differences < 1 dB at 200 kHz. Videos and photographs of the seafloor were used to ground truth interpretations of the *BS* curves. The results show that these *BS* curves measured with the echosounder are relevant for seabed classification and characterization. The different shapes and levels of *BS* when compared to ground truth are coherent with the Jackson model. The main limit of this prototype of echosounder is the signal to noise ratio, in particular for high frequency harmonics (≥ 400 kHz). The *in situ* calibration is unavoidable because of the non-linear parameter variations with water characteristics (temperature, salinity...). Calibrated *BS* curves from 100 kHz to 300 kHz can be directly compared to other measurements, for example to calibrate other instruments.

© 2021 Elsevier Ltd. All rights reserved.

1. Introduction

Single-beam echosounders (SBES) have been used since the 20th century primarily for hydrographic purposes. Their first aim was to achieve bathymetric requirements such as reliable detections of the seabed and precise positioning of the soundings. More recently,

they have also become reference systems for seabed characterization and classification mostly because of their usability (straight-forward technology, lightweight and portable), their ability to be fully calibrated using a sphere target [1] and their versatility in frequencies (available from 10 kHz to 500 kHz). Different algorithms have been developed to address the challenges, for example received pulse envelope alteration [2,3], or signal echo modification according to frequency [4]. However, seabed acoustic response depends on the frequency as well as the incidence angle [5–8]. Therefore, to be discriminant, the acoustic response of the seafloor

* Corresponding author.

E-mail address: irene.mopin@ensta-bretagne.org (I. Mopin).

must be measured according to several incident angles θ and transmitted frequencies f . This yields reflectivity or backscattering strengths $BS(f, \theta)$ specific of a seabed type [9].

In the context of traditional SBES, the angular issue is solved by mechanically tilting the system even if, obviously, the use of multi-beam echosounders would be more appropriate [10]. As for frequencies, transmitting a large diversity of frequencies implies the use of several systems (single- or multi-beams) on the same vessel, requiring larger vessels and increasing survey costs. Where the angular measurements are practicable, multi-frequency measurements are most often limited by space requirements on board [11]. In the case of MBES, new systems are able to transmit signals at different frequencies, but require either to run several acquisitions on the same survey line or to transmit alternatively one ping at one frequency at any single time. Signals are consequently not perfectly synchronised. Another method used for SBES is to transmit a signal containing several frequencies i.e. a frequency modulated (FM) signal. However, frequencies are also not in-phase and the bandwidth of a single head SBES is generally limited, restraining the diversity of frequency measurements available with one echo-sounder. The SBES presented in this paper is a compromise between the number of frequencies desired, the space available and the cost of the survey. Its ability to generate several spread frequencies (100 kHz apart) perfectly synchronised and with only one transducer head makes it efficient for seabed characterization or classification surveys and very economical of space.

The system is mechanically tilted to reach angles from 0° (nadir) to 60° , and designed to generate multiple frequencies perfectly simultaneously with a unique transducer head. The generation of these harmonic frequencies is based on the propagation medium's non-linear properties [12–14], producing frequencies multiples of the fundamental frequency transmitted (100 kHz, yielding harmonics at 200 kHz, 300 kHz, etc.). This approach is widely used in medical acoustics and non-destructive inspection [15] but seldom in underwater acoustics, even though the feasibility of characterizing underwater targets thanks to harmonic frequencies was demonstrated e.g. in [16].

Section 2 summarises the underlying theory and presents how it informed the design of transmitter and receivers, whose non-linear properties are measured in tanks and at sea. Section 3 explains how acoustic data is processed to get accurate seabed backscattering strengths $BS(f, \theta)$. Section 4 presents sea trials in the Bay of Brest (France) and compares the results with reference measurements from [17] and with established seabed response models like [18]. Finally, Section 5 discusses the need for *in situ* calibration and envisageable improvements.

2. Theory, design and validation of a harmonic single-beam echosounder

The non-linear properties of acoustic wave propagation in water [12,14] are used to generate multiple frequencies with a system classically employed in underwater acoustics: the SBES. The echosounder described in this paper is able to generate several isolated frequencies, harmonics of the lower one, perfectly simultaneous in time and space.

2.1. Using non-linearities in an underwater acoustics context

To generate several frequencies within a single transmitter, we take advantage of the non-linear propagation of acoustic waves in sea water [12,14]. The principle is based on the 3-D quadratic non-

linear equation for fluids in terms of the acoustic potential $\Phi(\mathbf{X}, t)$ [19,20]:

$$\Delta\Phi(\mathbf{X}, t) - \frac{1}{c_0^2} \frac{\partial^2 \Phi}{\partial t^2} = \frac{2}{c_0} \mathcal{A} \left(\frac{\partial \Phi}{\partial t} \right) + \frac{1}{c_0^2} \frac{\partial}{\partial t} \left[(\nabla \Phi)^2 + (\beta - 1) \frac{1}{c_0^2} \left(\frac{\partial \Phi}{\partial t} \right)^2 \right] \quad (1)$$

where \mathbf{X} are the 3-D coordinates and t the propagation time (omitted from the later expressions of Φ , to simplify the equation); c_0 is the sound speed in the given fluid (water), and β the non-linear coefficient [21,22]. $\mathcal{A}(\ast)$ is a linear operator related to attenuation. In water, it takes into account the thermoviscous attenuation $-\frac{b}{2\rho_0 c_0^3} \frac{\partial^2 \ast}{\partial t^2}$ [23], in which b is the viscosity coefficient and ρ_0 the density of the medium, and it also accounts for the relaxation [19,24].

As the acoustic wave propagates through water, non-linear processes will transfer some energy from the fundamental frequency to its harmonics [14,25,26]. To observe these non-linear phenomena, the power transmitted needs to be much higher than with traditional echosounders. This constraint is often a limitation to using non-linear acoustics. Previous studies and the model by [19,27] helped us to improve the development and design of the echosounder, making it efficient in terms of acoustic energy for each harmonic frequency.

2.2. Constraint on the transmitter: high power

According to [14], harmonic frequencies appear in the signal during its propagation through the medium, when only one single frequency is actually transmitted by the transducer. The main constraint, in practice, is that a very high acoustic level must be transmitted into the water, at the transducer head. Electronic components have therefore to be able to generate a high amplitude signal and the transducer itself must be designed to support such a high pressure variation on its surface, while avoiding cavitation and the generation of third harmonic when the transmitted signal is not sinusoidal. The transmitter (Tx) developed for this purpose is an 18 cm-diameter disk formed with composite-PZT [28], which resonates at 100 kHz (see Fig. 1). Its composition and large surface are enough to support high power at 100 kHz, allowing this fundamental frequency to be transmitted. The harmonic frequencies generated during propagation are therefore 200 kHz, 300 kHz, etc. The source level estimated from linear measurements of the transmitter sensitivity is 228.5 dB re. 1 μ Pa @ 1 m.

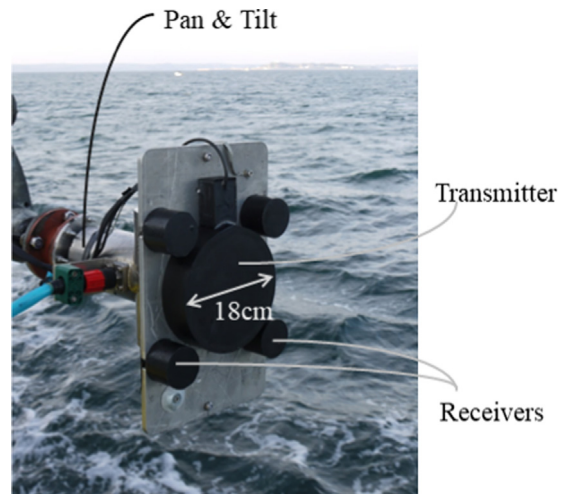


Fig. 1. Multi-frequency SBES before a survey, with one transmitting cylindrical transducer in the center, and four receivers spaced 20 cm apart.

2.3. Constraints on the receiver(s): the spread of frequencies

To receive all harmonic frequencies, the receivers must be wide-band. They also have to be very sensitive because the harmonic levels could be quite low (received seabed echo amplitude of the 300 kHz harmonic could be lower than 20 mV at 30 m range for a tilted angle of 60°), especially at very high frequencies. PVDF (Polyvinylidene fluoride) technology [29] respects these criteria and was consequently selected. We can note that with a suitable receiver sensitivity the range of the system is only limited by the level of the higher intended harmonic compared to the received noise level. The receivers (Rx) are in our case made of one layer of PVDF, with a backing formed by a layer of vinyl and a large syntactic foam as backing. They have the shape of a small disk 3 cm in diameter to optimise the sensitivity/aperture constraints at high frequencies. Four receivers are placed around the Tx transducer as shown on Fig. 1. Their vertical spacing is about 20 cm and is useful for seabed detection through interferometry.

2.4. Validation of harmonic frequencies generation

The effective generation of harmonic frequencies with the selected transducer shape and material is done by measuring the harmonic levels at several ranges from the transmitter in fully-controlled environments. These measurements were done in two tanks: one 10 m-long and filled with fresh water (at Sorbonne University, Paris, France), and one 35 m-long filled with sea water (at Ifremer, Brest, France). The experiments both consisted in emitting a continuous wave (CW) with the Tx transducer of Fig. 1 and receiving the direct-signal with a calibrated hydrophone Reson TC4034. Measurements were obtained every 2 or 3 meters in the small tank, and every 5 meters in the large tank. The level $L(r)$ of each harmonic, depending on the range r , is calculated after using a band-pass filter. Results are shown on Fig. 2. We can perfectly observe the creation of the harmonic along the range before the shock distance L_c [19] (around 2 m) where their levels are increasing. After the shock, the levels decrease with range, i.e. it is a transmission loss, mainly due to the geometrical divergence of the signal within the medium. The attenuation is close to negligible

on these short distances (around 3 dB/km in fresh water and 33 dB/km in salt water). We can notice a minute inflection at 10 m. This is explained by the different water conditions between each tank. The respective characteristics of these two environments are contrasted with conditions during the sea survey in Table 1.

These different sets of measurements show that, in each environment, the transmitter effectively and efficiently creates harmonic frequencies. The results also show the importance of knowing where the shock appears, i.e. when the harmonics are at their maximum levels. This is as important as knowing the far-field distance, in an operational point of view. Indeed, for ranges lower than L_c , measurements are not recommended as all the harmonic frequencies are not fully generated. This distance is therefore a characteristic of the multi-frequency echosounder and needs to be kept in mind by future users.

2.5. Directivity patterns and equivalent beam apertures

To estimate the reflectivity level of the seafloor at different incidence angles, we need to know the directivity pattern $D(f, r, \varphi)$ of the echosounder to calculate its equivalent beam aperture $\phi(f, r)$ for each frequency. The combined two-way directivity $10 \log(D(f, r, \varphi))$ is measured in the tanks for different ranges r from the echosounder and pointing angles $\varphi \in [-15^\circ; +15^\circ]$, and they are calculated for each frequency f . Fig. 3 shows the directivity patterns at $r = 20$ m for the fundamental frequency of 100 kHz and the first harmonics at 200 kHz and 300 kHz. We can observe the variations of the main beams' apertures according to frequency [31], and also asymmetries of the side-lobes, mainly due to the layout of the PZT component of the transducer (in spiral).

The equivalent aperture $\phi(f, r)$ of the echosounder is calculated for each frequency by integrating the corresponding measured directivity patterns [32] (Fig. 3). When measuring the directivity patterns for different r and plotting their equivalent apertures $\phi(f, r)$ we obtain the results of Fig. 4, showing the increase of beamwidths with range. At 100 kHz, they vary from 6.3° at 10 m to 6.8° at 30 m, at 200 kHz from 4.0° at 10 m to 4.6° at 30 m and at 300 kHz from 3.1° at 10 m to 3.9° at 30 m.

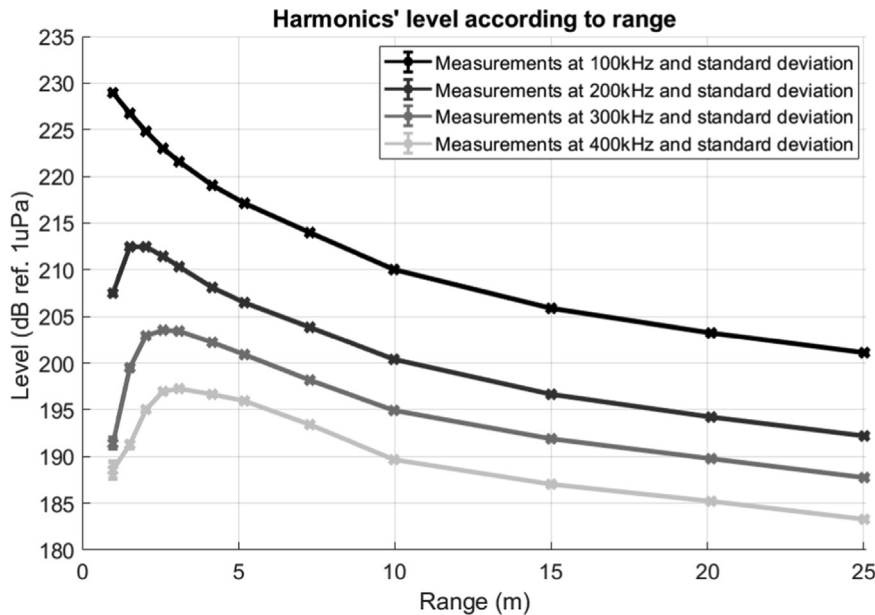


Fig. 2. Measurements of the generation of harmonic frequencies in a small (< 10 m) freshwater tank and in a large (≥ 10 m) salt water tank, according to the range from the transmitter with the maximum level at emission. At each range, 100 measurements are averaged. Associated standard deviations are not very noticeable because they are all < 0.9 dB.

Table 1

Characteristics of the water in the tanks and during the sea trials, measured *in situ*. The non-linear coefficient β is estimated with the empirical Blackstock formula [27,30] from the measurements of temperature and salinity. Because acoustics measurements in tanks were done horizontally i.e. the SBES axis crossed only one layer of water, the non-linear coefficient is constant during propagation. However, at sea, measurements are done vertically or while tilting the SBES, therefore its axis crossed several layers of water of different composition. The non-linear coefficient consequently varies during the propagation, and it is therefore given as a range of values.

	Small tank	Large tank	Survey at sea
Type of water	Fresh water	Salt water	Salt water
Sound speed (c_0)	1450 m/s	1498 m/s	[1500.8; 1503.0] m/s
Water density	1000 kg/m ³	1028 kg/m ³	[1026; 1027] kg/m ³
Temperature	9.8 °C	11.8 °C	[13.1; 13.8] °C
Salinity	0 psu	37 psu	[34.6; 35.4] psu
Particles in suspension	None	None	A lot
β (dimensionless)	Clear water 3.35	Clear water 3.59	Turbid water [3.59; 3.60]

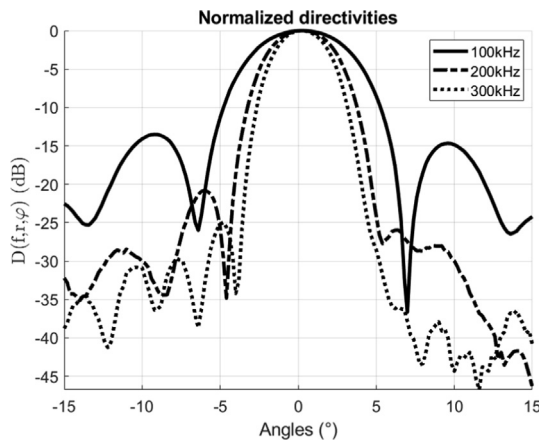


Fig. 3. Measured directivity patterns $10 \log(D(f, r, \phi))$ at $r = 20$ m for $f = 100$ kHz, $f = 200$ kHz, $f = 300$ kHz. At each angle, 4 measurements are averaged. Standard deviations σ stand in the following interval for each frequency: $\sigma_{100 \text{ kHz}}(\phi) \in [2.6; 6.1]$ dB, $\sigma_{200 \text{ kHz}}(\phi) \in [2.0; 7.3]$ dB, $\sigma_{300 \text{ kHz}}(\phi) \in [2.3; 6.7]$ dB.

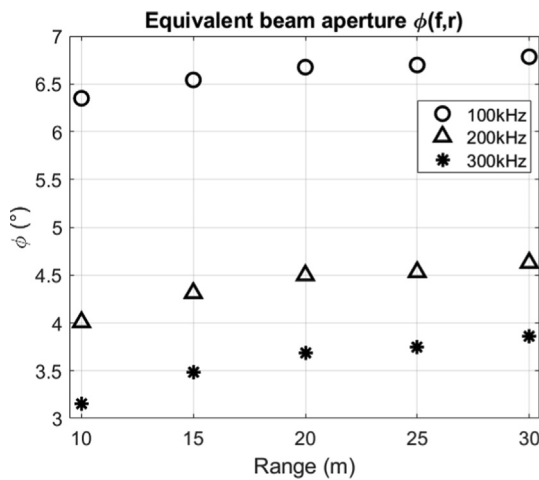


Fig. 4. Equivalent beam apertures $\phi(f, r)$ of the main lobe according to range and frequency, calculated from the directivity patterns measured between 10 m and 30 m.

2.6. Measurements of the operating gain and range variations

The echosounder aims to measure the absolute acoustic response of the seabed. It is therefore essential to evaluate: 1) its total operating gain according to frequency, $G(f)$, due to electrical connections, processing, etc., and: 2) the transmitted level to which

is directly related a specific decrease of each harmonic with range as observed in Section 2.4. In the case of backscatter measurements, we include both the transmit level and its decrease during two-way propagation, expressed as a variable noted $\mathcal{L}(f, r)$. Indeed, because of non-linear propagation, acoustic forward transmission losses $TL_{fw}(f, r)$ to the target differ from the classical, linear model (proportional to $20 \log r + \alpha r$ [32] with α the linear attenuation coefficient). Likewise, the operating gain cannot be calculated either with linear theoretical formulae [33].

For practical use, we propose to create look-up tables of each gain and frequency level according to the range: $G(f) + \mathcal{L}(f, r)$, that will be used to calculate the seabed response (sonar equation) in place of all the unknown parameters (see Eq. 2). This can be achieved with measurements on a calibrated target [34,1], moved along the axis of the echosounder. The principle is to compare the received backscattering level of the controlled point target with its actual target strength $TS(f)$ whose frequency spectrum is perfectly known [35]. The target used for our measurements is a full-metal sphere (tungsten, carbide and cobalt) of diameter 38.1 mm, chosen because its frequency responses have no anti-resonance at the frequencies we use (respectively 100 kHz, 200 kHz, 300 kHz). The final outcomes are look-up tables of $G(f) + \mathcal{L}(f, r)$ according to range and frequency. For our objective, the sphere is moved from 10 m to 30 m range which gives a sufficient range of look-up tables for surveys in the Bay of Brest (depths ≤ 30 m) (for larger ranges, the calibration should increase to similar ranges or, if the measurements could not be made because of practical reasons, an estimation of $G(f) + \mathcal{L}(f, r)$ variations for r greater than 30 m should be proposed, based on measurements at r lower than 30 m). For this experimental setup, the associated sonar equation is:

$$20 \log(V_{Rx}(f, r)) = 20 \log(V_{Tx}(f)) + S_h(f) + S_v(f) + 10 \log(D(f, r, \phi)) - TL_{fw}(f, r) - TL_{bw}(f, r) + TS(f) + G_o(f) \quad (2)$$

with f the harmonic frequency, V_{Rx} and V_{Tx} respectively the received and transmitted voltages, S_h and S_v respectively the receiver and transmitter sensitivities, $D(f, r, \phi)$ is the combined directivity function at transmission and reception, ϕ the angle in the beam (i.e. $D(f, r, \phi = 0^\circ) = 1$ on the beam-axis), TL_{fw} and TL_{bw} respectively the transmission losses forward (from the transmitter to the sphere) and backward (from the sphere to the receiver), and $G_o(f)$ encompasses the electrical gains. Because of the non-linear operation of the echosounder, the perfectly known parameters are only $V_{Rx}(f, r)$, the target strength of the sphere $TS(f)$ (i.e. its backscattering cross section [36]) and $D(f, r, \phi)$. Measurements on the target are done on the axis of the echosounder so that $10 \log(D(f, r, \phi)) = 0$. Consequently, we can define the difference $20 \log(V_{Rx}(f, r)) - TS(f)$ as the sum of an operating gain $G(f)$ and a level range variations $\mathcal{L}(f, r)$ such as:

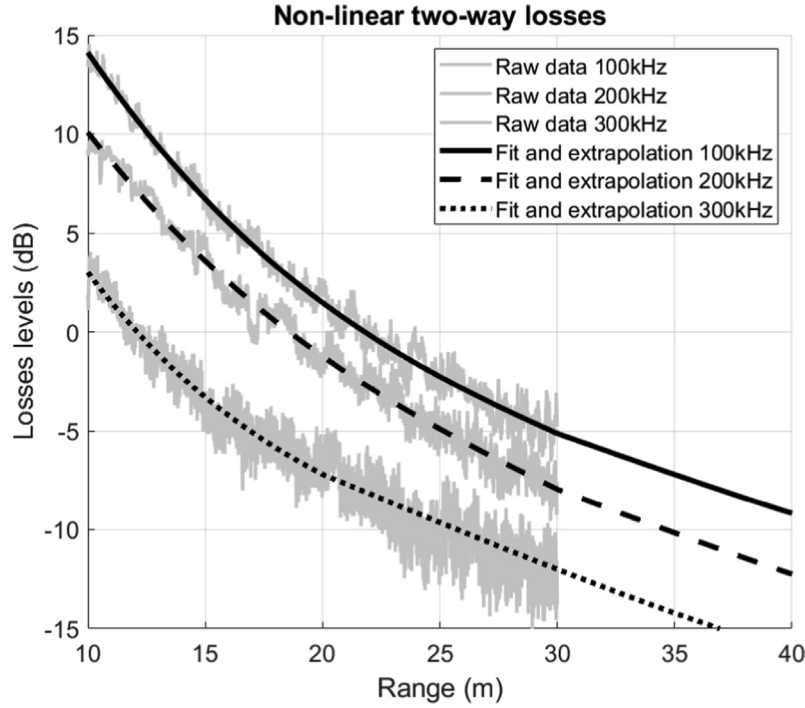


Fig. 5. Grey: measurements of $G(f) + \mathcal{L}(f, r)$ in the large tank of Ifremer (sea water) according to the range from the echosounder in operational mode (i.e. with the maximum level at emission). Black: best-fitting curves used as look-up tables.

$$G(f) + \mathcal{L}(f, r) = 20 \log(V_{Rx}(f, r)) - TS(f) \quad (3)$$

Measured $G(f) + \mathcal{L}(f, r)$ and their corresponding best-fitting curves used as look up tables are shown for the fundamental frequency and its 2 first harmonics on Fig. 5. Finally, $G(f) + \mathcal{L}(f, r)$ contains the propagation losses, Tx and Rx sensitivities, the fixed transmit level $20 \log(V_{Tx}(f))$, electrical gains, and signal processing gains of the echosounder we wished to estimate, and that will be useful for seabed reflectivity calculations.

3. Seabed reflectivity processing

Raw data from the multi-frequency echosounder are time-sampled values of received levels $20 \log(V_{Rx}(r))$, with $r = ct/2$, in which t is the listening time, i.e. the time after emission of the signal. Signals for each harmonic frequency are extracted thanks to a band-pass filter and noted $20 \log(V_{Rx}(f, r))$. The transmit signal, also called pulse, is a 100-kHz sine wave of duration T . Each harmonic received signal is perfectly in-phase and investigated separately. From these received time signals, the echo of the seabed is detected and its reflectivity index, or backscattering strength $BS(f, \theta)$, is computed (in decibels) as:

$$\begin{aligned} BS(f, \theta) = & 20 \log(V_{Rx}(f, r)) - 20 \log(V_{Tx}(f)) - S_h(f) - S_v(f) \\ & - 10 \log(D(f, r, \varphi)) + TL_{fw}(f, r) + TL_{bw}(f, r) - G_o(f) \\ & - 10 \log(A(f, \theta)) \end{aligned} \quad (4)$$

with θ the incidence angle on the seabed, $D(f, r, \varphi)$ the directivity (combining Tx and Rx) of the echosounder for the frequency f at the range r taken at the angle $\varphi = \cos^{-1}(h/r)$ the angle of the sample in the beam (with h the water height at nadir on a supposed flat seabed), $TL_{fw}(f, r)$ and $TL_{bw}(f, r)$ respectively the transmission losses forward (from the transmitter to the seabed) and backward (from the seabed to the receiver), and $A(f, \theta)$ the insonified area on the seafloor (see Section 3.2). Directivity patterns of the echosounder

$D(f, \varphi)$ for each frequency are also measured in the tanks with hydrophones, at varying range (their apertures slightly change during propagation). Using the look-up tables of $G(f) + \mathcal{L}(f, r)$ computed in Section 2.6, we can write:

$$BS(f, \theta) = G(f) + \mathcal{L}(f, r) - 10 \log(D(f, r, \varphi)) - 10 \log(A(f, \theta)) \quad (5)$$

where $r = h / \cos(\theta)$ is the flat seabed approximation linking r and θ .

3.1. Bottom echo detection

The sounding (i.e. the time-sample of the seafloor-echo coming from the center of the echo-sounder beam) is detected with two methods, depending on the incidence angle [17]: 1) on the center of gravity computed on the intensity values for angles near the nadir, 2) from phase differences, thanks to the receivers vertically aligned for other angles. The sounding range is noted r_s and its equivalent received time $t_s = 2r_s/c$. We can note that the seafloor echoes of the harmonic frequencies are in some cases very useful to improve detection (for example in case of phase ambiguities, due to the relatively large distance between two receivers). Indeed, the phase ramps at high frequencies are shorter and steeper than that of the fundamental frequency, because of their shorter beam-widths. Around the sounding sample, indexed by i , several time-samples are retained (this is the equivalent of the “snippets” of multibeam echosounders [37,38]). They are averaged to compute $BS(f, \theta)$ for one ping. As in [17], samples i are retained when the condition $\varphi_i \in [-1^\circ; +1^\circ]$ is valid with φ the angle of the samples in the beam.

3.2. Insonified area

The insonified area is calculated thanks to a geometrical model using the echosounder equivalent along-track ϕ_{al} and across-track ϕ_{ac} beam apertures [32], the incidence angle θ , and the effective pulse length T_{eff} (defined below) which takes into account the signal loss of energy during transmission. In our case, ϕ_{al} and ϕ_{ac} both

equal the equivalent beam aperture measured in Section 2.5 because of the SBES symmetry, i.e. $\phi_{al} = \phi_{ac} = \phi(f, r)$. The insonified area model is composed of two regimes, near-nadir and oblique-angle, such as [39] (assuming the slope along-track is flat):

$$A(f, \theta) = \min \left(\pi \frac{r^2}{\cos \theta} \left(\frac{\phi(f, r)}{2} \right)^2, \frac{c T_{\text{eff}}(f)}{2 \sin \theta} \cdot r \cdot \phi(f, r) \right) \quad (6)$$

The effective pulse lengths are computed for each frequency by measuring the difference of acoustic energy between the desired rectangular pulse and the pulse actually transmitted by the echosounder. Indeed, when the pulse is transmitted by the Tx transducer, its bandwidth creates transitory effects on the shape of the signal. The energy of the signal actually transmitted is therefore lower than the perfect rectangular pulse energy given electronically to the transducer. This difference of acoustic energy is taken into account by using an effective pulse length T_{eff} whose amplitude is unity and whose energy is proportional to the theoretical pulse energy by a factor called Sa_{corr} in [17,35], defined as:

$$10 \log(T_{\text{eff}}(f)) = 10 \log(T(f)) + Sa_{\text{corr}}(f) \quad (7)$$

with $T(f)$ the theoretical signal duration chosen by the user at $T(100 \text{ kHz}) = 600 \mu\text{s}$. Values of $Sa_{\text{corr}}(f)$ and $T_{\text{eff}}(f)$ are given in Table 2 for the fundamental frequency (100 kHz) and the first two harmonics (200 kHz and 300 kHz).

3.3. Resulting $BS(f, \theta)$ measurements

To estimate the backscattering strength (i.e. the $BS(f, \theta)$ curves) of a given seabed, the SBES has to be tilted mechanically to reach discrete incidence angles $\theta_j \in [0^\circ, 5^\circ, 10^\circ, \dots, 60^\circ]$. This is obtained with the pan & tilt device shown in Fig. 1. On a given surveyed area, 150 pings are recorded for each tilting angle. As recommended in [17], seabed samples i of each ping are retained to be part of a $BS(f, \theta_j)$ value (average) when their incidence angle on the seafloor $\theta_i = \theta_s + \phi_i + \gamma_s$ is included in the interval $[-1^\circ; +1^\circ]$ around the desired angles θ_j , i.e.:

$$BS(f, \theta_j) = 10 \log \left(\frac{1}{N} \sum_{i=1}^N \sigma_{BS}(f, \theta_i) \right) \text{ if } \theta_i \in [\theta_j - 1^\circ; \theta_j + 1^\circ] \text{ where } \theta_i = \theta_s + \phi_i + \gamma_s \quad (8)$$

with $\sigma_{BS}(f, \theta_i) = 10^{BS(f, \theta_i)/10}$, θ_s the incidence angle of the sounding on the seafloor ($\cos \theta_s = h/r_s$), ϕ_i the angle of the time-sample i in the beam (with respect to the axis), γ_s the roll values at the time of the sounding s , and N the number of samples i that respect the condition $\theta_i \in [\theta_j - 1^\circ; \theta_j + 1^\circ]$.

During our survey, the sea was perfectly calm (World Meteorological Organisation Sea State Code 0) and the roll of the ship was always $< \pm 1^\circ$ so that almost all values were averaged. We consequently obtain $BS(f, \theta)$ values for all incidence angles θ_j from 0° to 60° with a step of 5° .

3.4. Fitting the $BS(f, \theta)$ curves

In the following, the discrete measurements $BS(f, \theta_j)$ are fitted with the heuristical model GSAB (Generic Seafloor Acoustic

Backscatter) for seafloor backscattering strength [40], to get seabed $BS(f, \theta)$ curves that can be analysed in Section 4. The model describes the BS into three parts thanks to six parameters [41]:

$$BS(\theta) = 10 \log \left(A \cdot \exp \left(-\frac{\theta^2}{2B^2} \right) + C \cdot \cos^D(\theta) + E \cdot \exp \left(-\frac{\theta^2}{2F^2} \right) \right) \quad (9)$$

with A regulating the specular amplitude, B controlling the angular width of the specular regime, C giving the average backscatter level at oblique incidence, D being the angular decrement of the backscatter (equal to 2 for Lambert law), E the transitory maximum level and F its angular half-extent.

4. Sea trials and results

Sea trials took place in the Bay of Brest (France) in May 2016 aboard R/V *Thalia* of Ifremer. Three areas with distinct seafloor types (see Section 4.1) were surveyed in order to demonstrate the feasibility of discriminating seabeds with our echosounder. The SBES was mounted on a pole on the starboard side of the vessel (see Fig. 1). A pan&tilt system was used to tilt the sounder at several angles, from 0° (nadir) to 60° , with a 5° step. At each angle, data were acquired while the vessel was drifting slowly. This drift ensured a minimum of acoustic noise from the vessel's engines or electrical on-board devices, because the sounder was a prototype and therefore not fully fitted with filters against other types of acoustic noise. The calm weather during the survey ensured the vessel drifted for a distance short enough to assume the seafloor is the same for all pings.

4.1. Area descriptions

Measurements were done onto three areas of the Bay of Brest chosen for their distinct seabed types (see map on Fig. 6). Area 1 is at the mouth of the small Elorn river. Area 2 is in the so-called "Carré Renard", a plateau in the center of the Bay and also a well-surveyed area for echosounder calibration [17]. Finally, Area 3 is at the mouth of another small river, the Aulne. According to the morpho-sedimentological map in [42], created from [43,44], Area 1 is composed of "sandy mud" or "muddy sand", Area 2 is mostly composed of "gravels" with rare pebbles, and Area 3 is composed of "gravelly coarse sand" with maerl and episodic rocks. During the survey, videos and photographs of the seafloor were taken in these areas (cf. Fig. 7). They show sand and mud in Area 1, pebbles and brittle-stars in Area 2, and a hard seafloor (rock) and a large amount of shells in Area 3.

4.2. Raw results

The raw results take the form of several $BS(f, \theta)$ curves for frequencies of 100 kHz and above, for all 3 areas surveyed. At first, we compare on Fig. 8 the results at the fundamental frequency (100 kHz) for the different areas. Crosses, triangles and circles show the raw measurements (averages of acoustic intensity values) and lines show the fit of the GSAB model to these measurements. We observe differences in shape and level according to the areas, as expected. Area 3 has a hard and rough seafloor; correspondingly, the $BS(f, \theta)$ curve has a generally low level and is flattened at the nadir angles. Conversely, the curve of Area 1 (sandy/muddy seafloor) has a very large range of levels, from -6.4 dB at 0° to -26.8 dB at 60° , and a high specular level. The curve of Area 2 is in between those two descriptions, with a high global BS level but a medium range of BS values according to incidence angles and a visible specular regime, not as strong as Area 1. These effects of specular flattening are commonly observed [45–

Table 2

Proportionality coefficient $Sa_{\text{corr}}(f)$ between the theoretical pulse energy and the effective pulse energy, measured in the tanks for the fundamental frequency (100 kHz) and the first two harmonics (200 kHz and 300 kHz). Effective pulse lengths are associated to these values.

Frequencies	100 kHz	200 kHz	300 kHz
$Sa_{\text{corr}}(f)$	-0.37 dB	-0.49 dB	-1.03 dB
$T_{\text{eff}}(f)$	$551 \mu\text{s}$	$536 \mu\text{s}$	$473 \mu\text{s}$

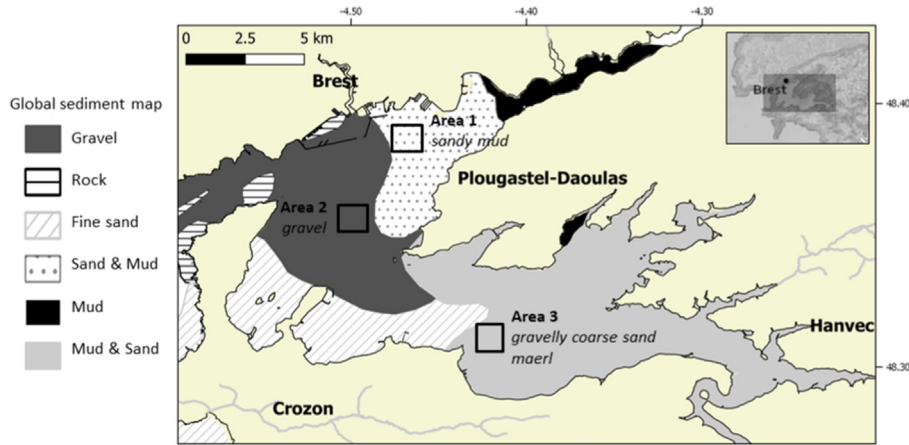


Fig. 6. Areas surveyed in the Bay of Brest (France). The global sediment map comes from data.shom.fr (www.shom.fr/HOM/GEOL_SEDIM_MONDIALE) and land information come from geo.data.gouv.fr. At the time of the survey, the water heights were constant for all pings: $h = 20.5$ m for Area 1, $h = 17$ m for Area 2, and $h = 31$ m for Area 3.

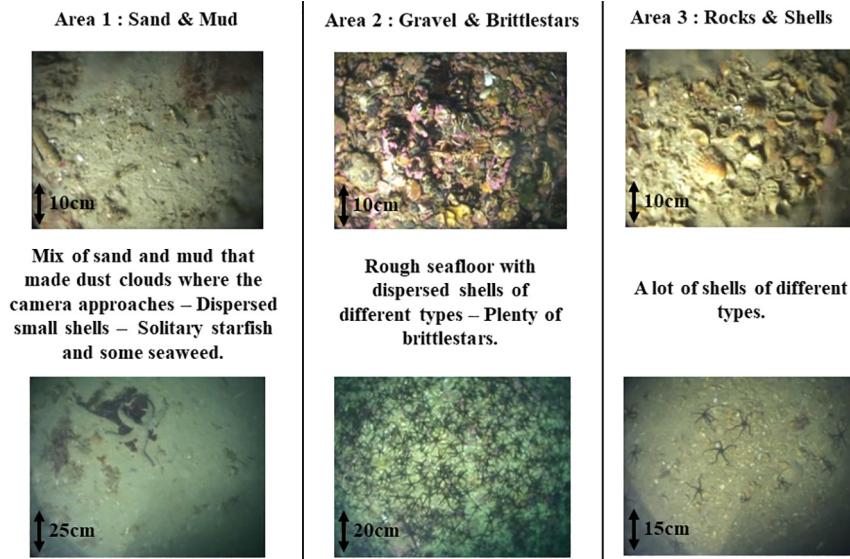


Fig. 7. Seafloor photographs in the three areas studied, taken during the survey, with visual descriptions. Data collected by the authors.

47] when the seabed rugosity changes from structures finer than the wavelength (like sand or mud at 100 kHz) to macrostructures close or larger than the wavelength (like pebbles or rocks). The specular shape can disappear, like for Area 3, on hard seafloor, as demonstrated e.g. by [18] (roughness effect).

We can also compare (see Fig. 9) raw results in one area for the fundamental frequency (100 kHz) with two of its harmonic frequencies (namely 200 kHz and 300 kHz). We observe frequency variations where, in particular, the shapes of the $BS(f, \theta)$ curves are modified, mostly on the specular parts which decrease with frequency and where Bragg backscattering [32] for grazing angles inversely increases.

4.3. Calibration on reference Area 2 ("Carré Renard")

Data were acquired in area 2 because it is a known reference area for echosounder calibration [17], and it was therefore possible to compare our results to reference curves noted $BS_{ref}(f, \theta)$. Our Ifremer colleagues kindly shared two reference curves at 200 kHz and 333 kHz, reported in [17]. Their 200-kHz curve $BS_{ref}(200 \text{ kHz}, \theta)$ can be usefully compared to our measurements

of $BS(200 \text{ kHz}, \theta)$. The 333-kHz curve can be used with caution to compare with our measurements at 300 kHz. The comparison is plotted as the difference $BS_{ref}(f, \theta) - BS(f, \theta)$ according to incidence angles for 200 kHz and 300 kHz respectively on Figure 10. We see that those differences follow a curve whose shape can be explained by several biases. The first one is visible in the range variations ($\mathcal{L}(f, r)$) estimated in Section 2.6, which can appear because of a difference in water composition (salinity) or turbidity between the measurements in the tanks and *in situ* (see Table 1) that may impact the generation of non-linearities [48,49] and therefore the levels of harmonic frequencies. The second bias is due to the difference of variation of β during the propagation. Indeed, the Tx signal propagates horizontally in the tanks and vertically or obliquely during the survey. Thus, whereas the non-linear coefficient is constant along the propagation in tank, it is variable *in situ*, introducing modification in the harmonic generation and sustain. A last bias comes from slight errors in the operating gain $G(f)$, from *in situ* sensitivity variations, electronics or processing adjustments. Thanks to the references curves, these biases can be quantified *in situ* and properly accounted for. Thus, the difference between the reference curve $BS_{ref}(f, \theta)$ and the raw-results for each inci-

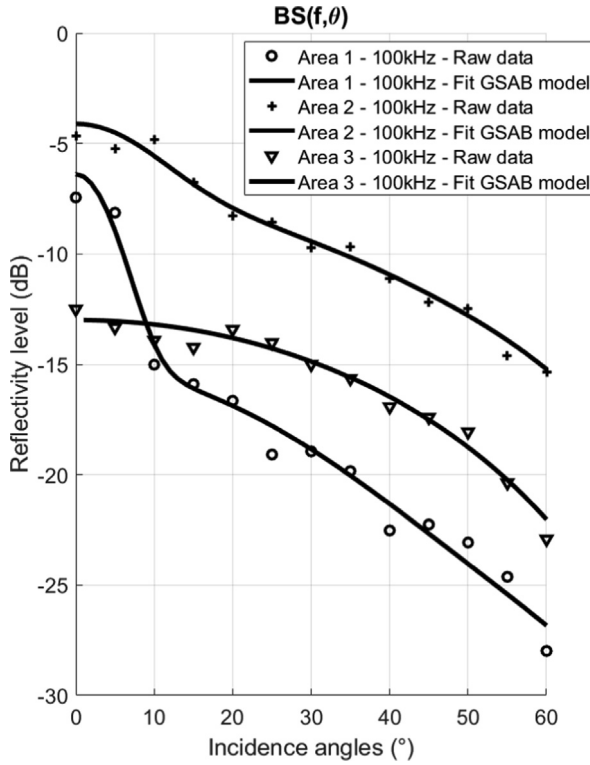


Fig. 8. $BS(f, \theta)$ curves of the fundamental frequency 100 kHz on the three areas surveyed: (1) sand & mud, (2) pebbles & brittle-stars, (3) hard seafloor (rocks) & shells. The raw measurements are respectively indicated with crosses, triangles and circles. The lines correspond to the respective GSAB model fits.

dependence angle $BS(f, \theta)$, noted $G_{corr}(f) + \mathcal{L}_{corr}(f, \theta) = BS_{ref}(f, \theta) - BS(f, \theta)$, is a correction which added to the $BS(f, \theta)$ calculation in Eq. 5, gives:

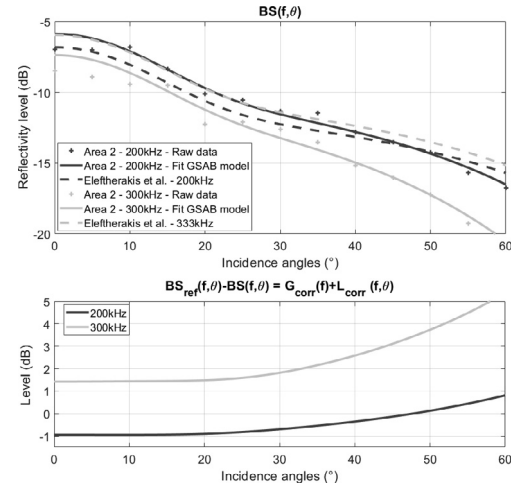


Fig. 10. Top: $BS(f, \theta)$ curves for harmonic frequency 200 kHz and 300 kHz on Area 2 (pebbles & brittle-stars). Raw measurements are indicated with crosses; the full line shows the GSAB model fit [32]; the dashed line corresponds to $BS_{ref}(200kHz, \theta)$ and $BS_{ref}(333kHz, \theta)$ curves from [17] on the same area. Bottom: gain and range variation corrections, i.e. differences $BS_{ref}(f, \theta) - BS(f, \theta) = G_{corr}(f) + \mathcal{L}_{corr}(f, \theta)$ between the reference reflectivity curve and the raw results.

$$BS_{calib}(f, \theta) = G(f) + G_{corr}(f) + \mathcal{L}(f, \theta) + \mathcal{L}_{corr}(f, \theta) - 10 \log(D(f, h/\theta, \varphi)) - 10 \log(A(f, \theta)) \quad (10)$$

The value $BS_{calib}(f, \theta)$ obtained after calibration on Area 2 is the absolute reflectivity level of this area. This calibration is done for the two frequencies of which reference reflectivity curves are available: 200 kHz and 300 kHz.

To apply the calibration to the other areas, we have to transform incidence angles to range, thanks to the measurements of echosounder altitude (i.e. the range h at nadir): $r = h / \cos(\theta)$. This gives a correction $G_{corr}(f) + \mathcal{L}_{corr}(f, r = h / \cos(\theta))$, function of range, and we can therefore calibrate the $BS(f, \theta)$ curves of each area by doing

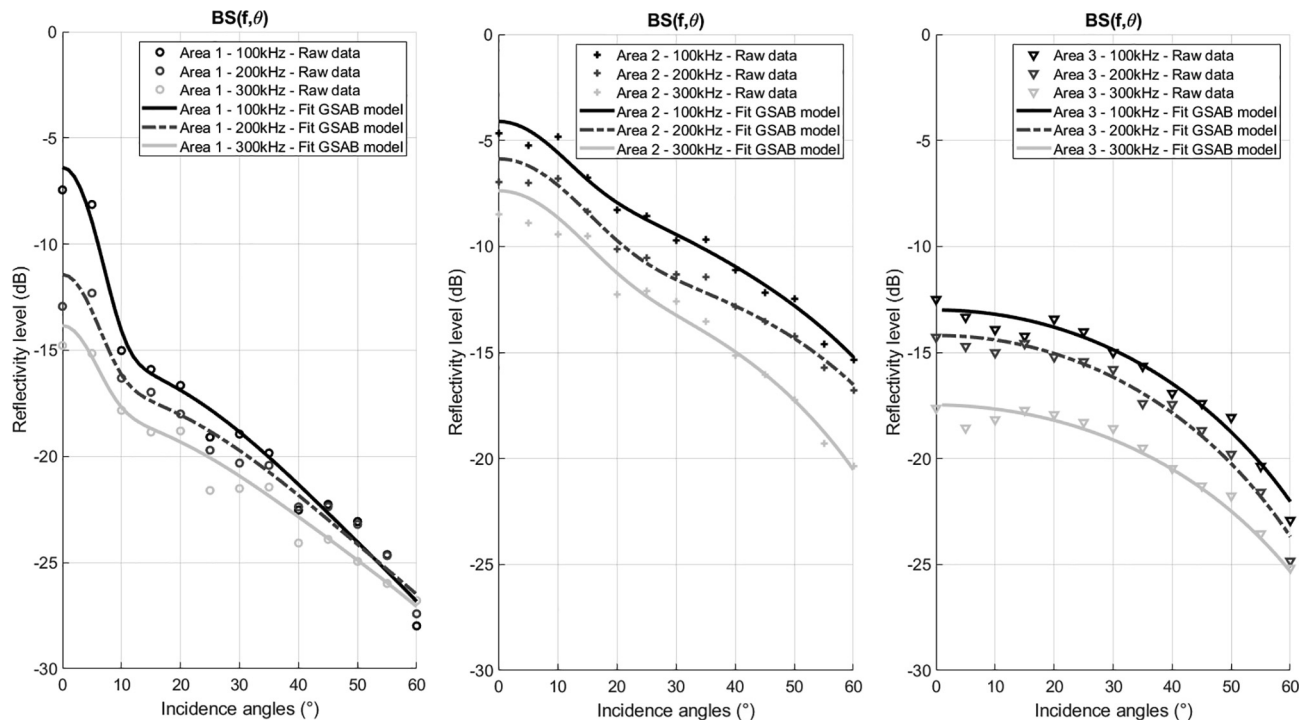


Fig. 9. $BS(f, \theta)$ curves of the fundamental frequency (100 kHz) and two harmonics (200 kHz and 300 kHz) on the three areas (left: sand & mud, center: pebbles & brittle-stars, right: hard seafloor (rocks) & shells). Raw measurements are indicated with circles and the GSAB model fits with lines.

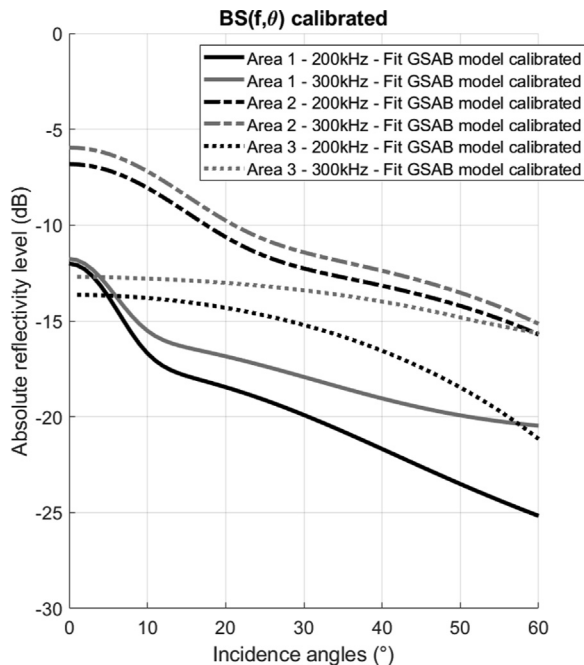


Fig. 11. Absolute $BS_{calib}(f, \theta)$ curves after calibration for the 3 areas and the two first harmonics 200 kHz and 300 kHz.

the same transformation. At the end, we obtain calibrated reflectivity curves of the three areas, shown in Fig. 11. We can see that the shapes of the curves discriminate clearly between the different seabed types, and also that the variations of those shapes for one area with frequency is not the same for each seabed type.

The raw results (Figs. 8 and 9) and the calibrated results (Fig. 11) allow us to conclude that the curves $BS_{calib}(f, \theta)$ obtained with the harmonic frequencies are able to discriminate seabed responses according to incidence angles and their absolute levels. Indeed, clear differences are observed between responses of seabed from the 3 areas surveyed that correspond to variations of the seabed composition. Also, modifications of the curve shape are observed between frequency responses like in Area 1 (sand & mud). These results clearly show the interest of multi-frequency single-beam echosounders for seabed characterization. They also demonstrate the importance of clearly mapping the characteristics of the instrument, in controlled tank environments and through a full and thorough calibration *in situ*.

5. Discussion

5.1. In situ calibration

The results of the calibration on the reference area show the clear necessity of a calibration *in situ* to obtain absolute reflectivity levels. Preliminary tank measurements are essential to characterise the entire instrument through parameters like its directivity, the effective pulse length, electrical gains, essential to calculate the backscattering strength. In our case, they were also extremely useful to validate the generation of harmonics, and determine the shock distance. The calibration is imperative to measure the true seabed acoustic responses of multiple areas, and ultimately this harmonic echosounder can be used as a reference system to calibrate other sounders, from single-beam to multibeam. An *in situ* calibration could be performed periodically in order 1) to check the validity of the last calibration results according to the new area

surveyed, and 2) to detect potential technical issues with the system (defective transducer, aging electronic, etc.).

5.2. Seafloor acoustic characterization and classification

Our prototype multi-frequency SBES uses non-linear acoustics to generate several harmonic frequencies. The seabed reflectivity variations presented in Section 4 as a function of incidence angles and for several frequencies are consistent with the physical considerations responses studied and modeled by Jackson in [47,50], even if the frequencies used in this article are mostly beyond the original validity domain of this model (up to 100 kHz) – other studies (e.g. [51,52]) already show it can be safely extended up to 240 kHz –: the acoustic response of a sandy-muddy seabed cover a large range of BS values from the nadir to the grazing angles and generate a strong specular effect, whereas a hard and rough seabed like rock has a flat response with a specular non-existent. These variations are found in our results (see Fig. 12) and give us confidence that classification and characterization of seabed types are feasible solutions with the harmonic single-beam echosounder. The frequency variations of the seabed responses are a major point for classification because it adds a lot of information. The possibility to measure several frequency responses simultaneously and therefore perfectly on the same seabed is a real asset of this type of echosounder.

5.3. Improving the non-linear echosounder

This multi-frequency SBES allows the concurrent use of three frequencies at once (central frequency of 100 kHz and two harmonics at 200 kHz and 300 kHz respectively), using a CW signal at transmission. By improving the system and specifically its signal-to-noise ratio, our next improvements will aim to access higher harmonics at 400 kHz, 500 kHz etc., providing more information on seabed types. The use of much higher frequencies (and therefore access to much smaller wavelengths) will also prove an asset for the imaging of less reflective targets like marine vegetation. Some types of macrophytes have limited gas content in their leaves and blades, but are detectable by using higher frequencies (≥ 400 kHz). This multi-frequency SBES, augmented with its pan & tilt system, can therefore prove very useful for studies of marine vegetation (in particular the mapping of canopy heights and the quantification of biomass) [53]. It can also be advantageously used for fisheries application, using the frequency-response of particular fish species or plankton (e.g. [54,55]). Other small-scale targets would also become more accessible, like gas bubbles in the water column above gas seeps or small oil inclusions in oil spills.

To be more efficient in measuring seabed acoustic responses curves, we can think, in future developments, about a system which could be able to generate beams simultaneously at a series of incident angles, such as a multi-beam echosounder [46], and following the first works at low frequency of [56,57].

6. Conclusion

The use of different technologies have enabled the development of a multi-frequency single-beam echo-sounder (SBES), using non-linear acoustics to transmit several harmonic frequencies. Our design generates a fundamental frequency at 100 kHz and several harmonic frequencies at 200 kHz and 300 kHz in particular. Bespoke, wide-band receivers were built to maximise backscatter measurements over ranges ≤ 30 m, commensurate with the depths expected in field surveys. The generation of harmonic frequencies was checked and quantified through tank experiments.

A complete processing methodology was presented, enabling to fully calibrate the echosounder, and we showed the importance of *in situ* calibration to account for variability in the marine environments. Mounted on a pan & tilt unit, the SBES is able to measure absolute seafloor reflectivity $BS_{\text{calib}}(f, \theta)$, according to incident angles and to different frequencies, at the same time and for the exact same patch of seabed. The multi-frequency SBES was tested in a survey in the Bay of Brest (France), measuring different types of seabed concurrently imaged with seafloor photographs and videos. One of the areas ("Carré Renard") benefited from previous measurements, and we were able to demonstrate the consistency of the different measurements, matching seabed types and differences. These results prove that acoustic seafloor characterization and classification is possible with this kind of instrument.

Declaration of Competing Interest

The authors declare that they have no known competing financial interests or personal relationships that could have appeared to influence the work reported in this paper.

Acknowledgments

This research was supported by the Direction Générale de l'Armement (DGA) and Agence Nationale de la Recherche (ANR) in France (project ANR-14-ASTR-0022). IM's PhD studentship is funded by the Agence Innovation Défense (AID) in France and the Defence Science Technology Laboratory (DSTL) in the UK (project #2018632). We would like to thank Ifremer for their help with the tank measurements and the survey with R/V *Thalia*.

References

- [1] Demer DA, Berger L, Bernasconi M, Bethke E, Boswell K, Chu D, et al. Calibration of acoustic instruments. ICES Cooper Res Rep 2015;326(133). <https://doi.org/10.25607/OBP-185>.
- [2] Pouliquen E, Lurton X. Seabed identification using echo-sounder signals. In: European Conference on Underwater Acoustics, Elsevier Applied Science, London and New York; vol. 535. 1992, p. 14–8.
- [3] Snellen M, Siemes K, Simons DG. Model-based sediment classification using single-beam echosounder signals. J Acoust Soc Am 2011;129(5):2878–88. <https://doi.org/10.1121/1.3569718>.
- [4] Hamilton L, Mulhearn P, Poeckert R. Comparison of ROXANN and QTC-View acoustic bottom classification system performance for the Cairns area, Great Barrier Reef, Australia. Continental Shelf Res 1999;19(12):1577–97. [https://doi.org/10.1016/S0278-4343\(99\)00020-5](https://doi.org/10.1016/S0278-4343(99)00020-5).
- [5] De Moustier C. Beyond bathymetry: Mapping acoustic backscattering from the deep seafloor with Sea Beam. J Acoust Soc Am 1986;79(2):316–31. <https://doi.org/10.1121/1.393570>.
- [6] Clarke JH, Danforth B, Valentine P. Areal seabed classification using backscatter angular response at 95kHz. High Frequency Seafloor Acoustics 1997; SACLANTCEN Conference Proceedings CP-45:243–250.
- [7] Brown CJ, Blondel P. Developments in the application of multibeam sonar backscatter for seafloor habitat mapping. Appl Acoust 2009;70(10):1242–7. <https://doi.org/10.1016/j.apacoust.2008.08.004>. the Application of Underwater Acoustics for Seabed Habitat Mapping.
- [8] Hughes Clarke J. Toward remote seafloor classification using the angular response of acoustic backscattering: a case study from multiple overlapping glacia data. IEEE J Ocean Eng 1994;19(1):112–27. <https://doi.org/10.1109/48.289456>.
- [9] Innangi S, Barra M, Di Martino G, Parnum I, Tonielli R, Mazzola S. Reson seabat 8125 backscatter data as a tool for seabed characterization (central mediterranean, southern Italy): Results from different processing approaches. Appl Acoust 2015;87:109–22. <https://doi.org/10.1016/j.apacoust.2014.06.014>.
- [10] Fezzani R, Berger L. Analysis of calibrated seafloor backscatter for habitat classification methodology and case study of 158 spots in the Bay of Biscay and Celtic Sea. Mar Geophys Res 2018;39(1–2):169–81.
- [11] Pouliquen E, Zerr B, Pace NG, Spina F. Seabed segmentation using a combination of high frequency sensors. In: Oceans '99. MTS/IEEE. Riding the Crest into the 21st Century. Conference and Exhibition. Conference Proceedings (IEEE Cat. No.99CH37008); vol. 2. 1999, p. 888–93. doi: 10.1109/OCEANS.1999.804991.
- [12] Bulanov V, Korskov I, Popov P. Measurements of the nonlinear acoustic parameter of sea water via a device using reflected pulses. Instrum Exp Technol 2017;60(3):414–7.
- [13] Endo H. Calculation of nonlinearity parameter for seawater. J Acoust Soc Am 1984;76(1).
- [14] Rudnick I. On the attenuation of finite amplitude waves in a liquid. J Acoust Soc Am 1958;30(6):564–7. <https://doi.org/10.1121/1.1909686>.
- [15] Bjørnø L. Forty years of nonlinear ultrasound. Ultrasonics 2002;40(1):11–7. [https://doi.org/10.1016/S0041-624X\(02\)00084-7](https://doi.org/10.1016/S0041-624X(02)00084-7).
- [16] Prieur F, Nasholm SP, Austeng A, Tichy F, Holm S. Feasibility of second harmonic imaging in active sonar: Measurements and simulations. IEEE J Ocean Eng 2012;37(3):467–77. <https://doi.org/10.1109/OE.2012.2198933>.
- [17] Eleftherakis D, Berger L, Le Bouffant N, Pacault A, Augustin JM, Lurton X. Backscatter calibration of high-frequency multibeam echosounder using a reference single-beam system, on natural seafloor. Mar Geophys Res 2018;39(1–2):55–73.
- [18] Jackson D. APL-UW high-frequency ocean environmental acoustic models handbook. Tech. Rep. 102; University of Washington; 1994.
- [19] Di Marcorberardino L, Marchal J, Cervenka P. Nonlinear multi-frequency transmitter for seafloor characterization. Acta Acust united Acust 2011;97(2):202–8.
- [20] Hamilton MF, Blackstock DT. Nonlinear acoustics. Academic Press; 1997.
- [21] Fox FE, Wallace WA. Absorption of finite amplitude sound waves. J Acoust Soc Am 1954;26(6):994–1006. <https://doi.org/10.1121/1.1907468>.
- [22] Beyer RT. Parameter of nonlinearity in fluids. J Acoust Soc Am 1960;32(6):719–21. <https://doi.org/10.1121/1.1908195>.
- [23] Kuznetsov V. Equations of nonlinear acoustics. Sov Phys Acoust 1971;16:467–70.
- [24] Pierce AD. Acoustics: An introduction to its physical principles and applications. 1989 Edition. Acoustical Society of America; 1990.
- [25] Enflo BO, Hedberg CM. Theory of nonlinear acoustics in fluids, vol. 67. Springer Science & Business Media; 2006.
- [26] Beyer RT. Nonlinear acoustics. Phys Acoust 2012;2(Part B):231–332.
- [27] Marchal J. Acoustique non linéaire: contribution théorique et expérimentale à l'étude de l'émission paramétrique (Non-linear acoustics: theoretical and experimental contribution to the parametric transmission research). Ph.D. thesis; Paris 6; 2002.
- [28] Ting RY. A review on the development of piezoelectric composites for underwater acoustic transducer applications. IEEE Trans Instrum Meas 1992;41(1):64–7. <https://doi.org/10.1109/19.126633>.
- [29] Woodward B, Chandra R. Underwater acoustic measurements on polyvinylidene fluoride transducers. Electrocomponent Sci Technol 1978;5. <https://doi.org/10.1155/APEC.5.149>.
- [30] Blackstock DT. Basic research in nonlinear acoustics. Texas Univ., Austin Report; 1975.
- [31] Blackstock DT. Nonlinear acoustics: Propagation in a periodic waveguide, scattering of sound by sound, propagation through a three-layer fluid, and nonlinearity parameters of sea water. Tech. Rep.; Texas Univ. at Austin Applied Research Labs; 1991.
- [32] Lurton X. An Introduction to Underwater Acoustics. Principles and Applications. Springer; 2010.
- [33] Sherman CH, Butler JL. Transducers and arrays for underwater sound, vol. 4. Springer; 2007.
- [34] Simmonds J, MacLennan DN. Fisheries acoustics: theory and practice. John Wiley & Sons; 2008.
- [35] Ona E, Mazauric V. Calibration LNA. methods for two scientific multibeam systems. ICES J Mar Sci 2009;66:1326–34.
- [36] Foote KG. Optimizing two targets for calibrating a broadband multibeam sonar. In: OCEANS 2006. p. 1–4. <https://doi.org/10.1109/OCEANS.2006.306944>.
- [37] Schimel AC, Beaudoin J, Parnum IM, Le Bas T, Schmidt V, Keith G, et al. Multibeam sonar backscatter data processing. Mar Geophys Res 2018;39(1):121–37.
- [38] Lucieir V, Picard K, Siwabessy J, Jordan A, Tran M, Monk J. Seafloor mapping field manual for multibeam sonar [Version 1]. Field Manuals for Marine Sampling to Monitor Australian Waters, Version 1 2018; Canberra, Australia. NESP Marine Biodiversity Hub:42–64. <https://doi.org/10.11636/9781925297669>.
- [39] Malik M, Lurton X, Mayer L. A framework to quantify uncertainties of seafloor backscatter from swath mapping echosounders. Mar Geophys Res 2018;39(1–2):151–68.
- [40] Lamarche G, Lurton X, Verdier AL, Augustin JM. Quantitative characterisation of seafloor substrate and bedforms using advanced processing of multibeam backscatter – Application to Cook Strait, New Zealand. Continental Shelf Research 2011;31(2, Suppl):S93–S109. doi: 10.1016/j.csr.2010.06.001; geological and Biological Mapping and Characterisation of Benthic Marine Environments.
- [41] Lurton X, Lamarche G, Brown C, Lucieir V, Rice G, Schimel A, et al. Backscatter measurements by seafloor-mapping sonars: guidelines and recommendations. In: A collective report by members of the GeoHab Backscatter Working Group.
- [42] Gregoire G. Dynamique sédimentaire et évolution holocène d'un système macrotidal semi-fermé: l'exemple de la rade de Brest. (Sedimentary dynamics and holocen evolution of a macrotidal half-closed system: the example of the bay of Brest)). Ph.D. thesis; Institut français de recherche pour l'exploitation de la mer; 2016. URL: <http://www.theses.fr/2016BRES0103>.
- [43] Gregoire G, Ehrhold A, Roy PL, Jouet G, Garlan T. Modern morpho-sedimentological patterns in a tide-dominated estuary system: the Bay of Brest (west Brittany, France). J Maps 2016;12(5):1152–9. <https://doi.org/10.1080/17445647.2016.1139514>.

- [44] Pluquet F, Ehrhold A. Une nouvelle stratégie d'étude des habitats marins littoraux au moyen de la vedette acoustique V/O Haliotis. (A new study strategy of coastal marine habitats with research vessel R/V Haliotis). Tech. Rep.; Ifremer/DYNECO/EB/09-02/FP; 2009.
- [45] Kloser R, Penrose J, Butler A. Multi-beam backscatter measurements used to infer seabed habitats. *Continental Shelf Res* 2010;30(16):1772–82. <https://doi.org/10.1016/j.csr.2010.08.004>.
- [46] Fonseca L, Brown C, Calder B, Mayer L, Rzhannov Y. Angular range analysis of acoustic themes from stanton banks ireland: A link between visual interpretation and multibeam echosounder angular signatures. *Appl Acoust* 2009;70(10):1298–304. <https://doi.org/10.1016/j.apacoust.2008.09.008> [the Application of Underwater Acoustics for Seabed Habitat Mapping].
- [47] Jackson DR, Winebrenner DP, Ishimaru A. Application of the composite roughness model to high-frequency bottom backscattering. *J Acoust Soc Amer* 1986;79(5):1410–22. <https://doi.org/10.1121/1.393669>.
- [48] Kim BN, Yoon SW. Nonlinear parameter estimation in water-saturated sandy sediment with difference frequency acoustic wave. *Ultrasonics* 2009;49(4):438–45. <https://doi.org/10.1016/j.ultras.2008.11.002>.
- [49] Akulichev V, Bulanov V. Acoustical nonlinearity, sound absorption, and scattering in bubble-saturated seawater. In: *Doklady Earth Sciences*; vol. 479. Springer; 2018, p. 375–8.
- [50] Jackson DR, Baird AM, Crisp JJ, Thomson PAG. High-frequency bottom backscatter measurements in shallow water. *J Acoust Soc Am* 1986;80(4):1188–99. <https://doi.org/10.1121/1.393809>.
- [51] Choi JW, Na J, Seong W. 240-khz bistatic bottom scattering measurements in shallow water. *IEEE J Oceanic Eng* 2001;26(1):54–62. <https://doi.org/10.1109/48.917926>.
- [52] Blondel P, Dobbins PF, Jayasundere N, Cosci M. High-frequency bistatic scattering experiments using proud and buried targets. In: *Acoustic Sensing Techniques for the Shallow Water Environment*. Springer; 2006. p. 155–70.
- [53] Tegowski J, Kruss A, Tatarek A, Wiktor J, Blondel P. Spatial distribution of macroalgae along the shores of Kongsfjorden (West Spitsbergen) using acoustic imaging. online; 2017. doi: 10.1515/popore-2017-0009.
- [54] Stanton TK, Chu D, Jech JM, Irish JD. New broadband methods for resonance classification and high-resolution imagery of fish with swimbladders using a modified commercial broadband echosounder. *ICES J Mar Sci* 2010;67(2):365–78. doi: 10.1093/icesjms/fsp262. arXiv:<https://academic.oup.com/icesjms/article-pdf/67/2/365/29136431/fsp262.pdf>.
- [55] Lavery AC, Chu D, Moum JN. Measurements of acoustic scattering from zooplankton and oceanic microstructure using a broadband echosounder. *ICES J Mar Sci* 2009;67(2):379–94. doi: 10.1093/icesjms/fsp242. arXiv:<https://academic.oup.com/icesjms/article-pdf/67/2/379/29135889/fsp242.pdf>.
- [56] Marchal J, Cervenka P. Modeling of the parametric transmission with the spatial Fourier formalism. *Optimization of a parametric antenna. Acta Acustica united with Acustica* 2004;90(1):49–61.
- [57] Foulon M, Amate M, Burlet N, Penven P, Cervenka P, Marchal J. Experimentations and sonar development for buried objects detection and classification. Tech. Rep.; Institut Jean Le Rond D'Alembert; 2011.